

INTERACTION OF LASER RADIATION WITH MATTER

PACS numbers: 79.20.Eb; 42.65.Jx; 42.65.Re
DOI: 10.1070/QE2015v045n08ABEH015515

Femtosecond-laser fabrication of cyclic structures in the bulk of transparent dielectrics

S.K. Vartapetov, D.V. Ganin, K.E. Lapshin, A.Z. Obidin

Abstract. **We report the results of the experiments on developing precision micromachining technology, obtained under the conditions of focusing the pulses of a femtosecond (FS) laser into the volume of a transparent material, which is important, particularly, in the processing of biomaterials in ophthalmology. The implementation conditions and some characteristic features of the special regime of micromachining are determined, when at a definite relation between the sample scanning velocity and the repetition rate of FS pulses the region, destroyed by the laser radiation, is shifted along the optical axis towards the objective and back, forming cyclic patterns inside the sample. It is supposed that the main causes of the damage region shift are the induced modification of the refractive index and the reduction of the damage threshold due to the change in the material density and structure in the microscopic domain, adjacent to the boundary of the cavity produced by the previous pulse. The results of the performed study with the above regime taken into account were used in the technology of precision cutting of crystals, glasses and polymers. The best quality of the cut surface is achieved under the conditions, eliminating the appearance of the cyclic regime. In the samples of polycarbonate, polymethyl methacrylate and fused silica the cylindrical cavities were obtained with the aspect ratio higher than 200, directed along the laser beam, and microcapillaries with the diameter 1–2 μm in the direction, perpendicular to this beam.**

Keywords: *femtosecond laser pulse, microstructures, filament, interaction of femtosecond radiation with transparent dielectrics, photodestruction, focusing into the bulk of material.*

1. Introduction

Femtosecond (FS) lasers are a preferable instrument for nano- and micromachining of materials, fabrication of photonic and fluidic devices, e.g., waveguides, couplers, optoelectronic systems and microcapillaries [1] based on the transparent polymers, glasses and fused silica [2–5]. Since the demonstration of high precision of processing different biomaterials by means of FS lasers, a real possibility has appeared to use them in ophthalmology for correcting the cornea curvature and cataract removal.

Polymers, glasses and biomaterials have very small linear absorption in the near-IR range, but under tight focusing of radiation they demonstrate strong nonlinear absorption. In the region of the focal waist of the objective this leads to the formation of a plasma microchannel, to the change in refractive index Δn at the axis and in the vicinity of the microchannel and, finally, to the optical breakdown and material microdestruction [6–10]. Since all these processes have strongly nonlinear, and, therefore, threshold behaviour, one can achieve sub-diffraction quality of the material machining by choosing the intensity slightly above the threshold value for a given process. The advantage of this method is the possibility of a local impact on small (a few cubic micrometres in volume) zones inside the transparent samples, not affecting the adjacent regions, including those in which the radiation propagates.

Recently, a number of papers reported the formation of cavities inside SiO_2 samples with prescribed nanoscale parameters using a FS laser [11, 12]. Toratani et al. [13] report the formation of cavities with the diameter $d \sim 200$ nm and the length $l \sim 20$ μm at the depth 20–70 μm. It is assumed that the origin of such high-aspect ($l/d \gg 1$) cavities and their characteristics are related to self-focusing of the FS pulse in silica. The influence of heat accumulation on the variation of the refractive index Δn in the focal waist region at high repetition rates of the FS pulses is studied in Refs [14, 15]. The formation of prolate microcavities under the action of FS pulses due to fast compaction of the material, leading the local rupture in the interaction region, was demonstrated in Ref. [16], and was also explained by the self-focusing effect.

Besides self-focusing, an important role for the formation of cavities and filaments with changed refractive index, strongly prolate in the beam direction, is played by the longitudinal spherical aberration (SA) that can essentially modify the intensity distribution profile in the focal waist [17, 18]. Sun et al. [19] investigated the influence of the so-called intrinsic SA, the self-focusing effect, and the longitudinal (interface) SA arising at the air–glass interface, on the length of the plasma channel (filament) luminescence in SiO_2 samples into which the FS pulses were focused. The presence of the capillary effect, as well as the measurements carried out with a scanning electron microscope (SEM), confirmed that the micromodification inside the sample having the form of a filament is a cylindrical cavity with the surface of rather high quality [20, 21].

To solve many problems the high-precision focusing of the laser radiation energy into the microregions inside the processed object is necessary. However, in the presence of longitudinal spherical aberrations the shape of intra-volume microdamages under the FS micromachining can strongly differ from the spherical one and have the form of filaments, the shape and size of which depend on the parameters of the FS laser, the sample and the experimental conditions [19, 22].

S.K. Vartapetov, D.V. Ganin, K.E. Lapshin, A.Z. Obidin Physics Instrumentation Center, A.M. Prokhorov General Physics Institute, Russian Academy of Sciences, Troitsk, 142190 Moscow, Russia; e-mail: svart@pic.troitsk.ru

Received 8 April 2014; revision received 2 December 2014
Kvantovaya Elektronika **45** (8) 725–730 (2015)
Translated by V.L. Derbov

The aim of this work was to determine the conditions of the phenomenon, insufficiently studied earlier and consisting in the following: in transparent dielectrics the region of microdestruction, formed by the focused FS laser radiation, experiences a self-induced depth displacement towards the objective and back, forming intra-sample cyclic patterns with a set of characteristic features. The study of technology of formation and suppression of such structures and the demonstration of the possibility to use the obtained results in the material processing is also the aim of the paper.

2. Experimental setup, samples, experimental techniques

The schematic diagram of the experiment is presented in Fig. 1a. Femtosecond pulses were generated by a RYF-10/35 laser system ('Avesta-Project') with the following parameters of radiation: the wavelength 1025 nm, the pulse repetition rate f from 1 Hz to 2 kHz, the pulse energy 150 μJ, the pulse duration smaller than 350 fs, the diameter of the output beam 3.2 mm at the 1/e level of intensity.

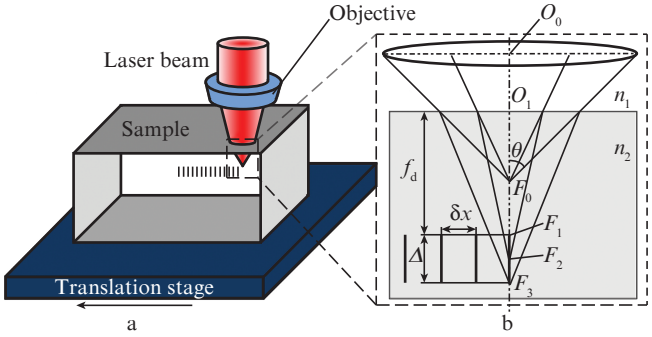

Figure 1. Schematic diagram of focusing the FS pulses into the sample volume (a) and the paths of the focused rays (b); F_0 is the geometric focus in air; F_1 is the focal point in the paraxial approximation, $f_d = nO_1F_0$ is the focusing depth, F_3 is focal point of peripheral rays, $\Delta = f_d/n[(n^2 - \mathrm{NA}^2)/(1 - \mathrm{NA}^2) - n]^{1/2}$ is the focal waist length with the spherical aberration at the boundary between the sample and air taken into account [19], δx is the separation between the centres of the focusing spots.

The energy of the pulses was controlled with an attenuator, consisting of a half-wave plate and a polariser. The laser beam width was expanded using a VIS-YAG 4X telescope (LINOS) with the magnification 4×.

In the experiment we used a 54-18-23-1064 objective (Special Optics) with NA = 0.39. The objective was mounted on the z-translation stage, which made it possible to control the depth of the radiation focusing into the sample, mounted perpendicular to the beam on the 8MT173-50 x–y translation stage (Standa) that had the maximal scanning velocity up to 800 μm s^{-1}. To measure the power a PD 300-1W detector (350–1100 nm) and a Nova power meter (Ophir Photonics) were used.

In the experiments we used the samples of polycarbonate (PC) in the form of plates with the dimensions 50×20×3 mm with polished faces. Figure 2 presents the photographs of the FS pulse impact traces in the form of a comb of tracks with different length. The laser beam is incident from above; the sample is shifted perpendicular to the beam. Each region of the damage (filament) corresponds to a single pulse. It is seen

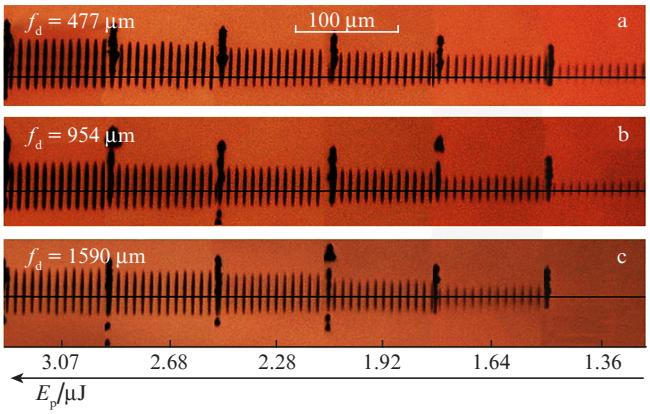

Figure 2. Filaments, produced by irradiation of PC with FS pulses at different focusing depths f_d (horizontal line) and energies E_p; NA = 0.39 (side view).

that the filaments are separated from each other and have high contrast. The photographs were obtained using a NIKON LV100D microscope. The diameter of the filament cross section at the half of their length amounted to 2 ± 0.05 μm. The filament-shaped destruction was clearly observed at the radiation intensities $I \sim 8 \times 10^{13}$ W cm^{-2}, the threshold point-like destructions were observed at $I \sim (1-2)\cdot 10^{13}$ W cm^{-2}. During the pause between the pulses $\tau = 10^{-2}$ s (f = 100 Hz) for the sample displacement velocity v_{sc} = 800 μm s^{-1} the sample shifts by the step $\delta x = v_{sc}/f$, which yields 8 μm, and after 12 such steps the samples stops. In the next series of 12 steps (96 μm) the pulse energy is increased. Thus, the series, separated by the 'standing points' (v_{sc} = 0) yield filament combs, created at the constant depth of focusing f_d with pulses of different energy for each individual segment. The processing of the photograph has shown that the filament length grows with increasing pulse energy, and Δ varies according to the near linear law ($\Delta \propto f_d$).

In the centre of Fig. 3 the side view of an individual filament is presented, as well as several its cross sections, observed in crossed polarisers and in natural light. It is seen that in the vicinity of the destructed region the ring-shaped area has greater brightness; in turn, this area is surrounded by the zone of smaller brightness, as compared to the background illumi-

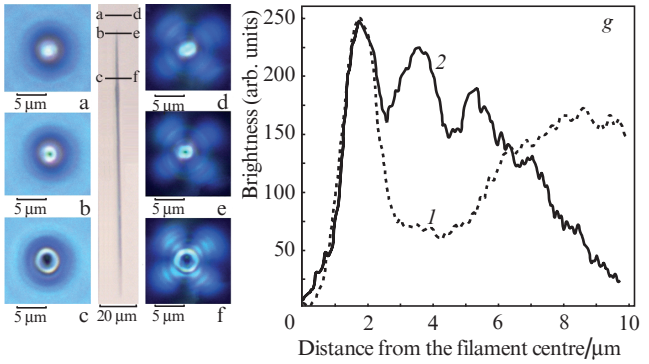

Figure 3. Microphotographs of a single filament and its cross sections in natural light [curve (*1*); a, b, c] and in crossed polarisers [curve (*2*); d, e, f]; dependence of the brightness on the distance from the filament centre (g), plotted using the photographs (c) and (f).

nation (Figs 3b and 3c). The ring-shaped structure is observed along the entire filament. This may be due to the change in the refractive index in the vicinity of the filament and, as a consequence, the additional focusing of the next pulse into the zone located closer to the objective. Figures 3d–f show the optical anisotropy in the vicinity of the filament, indicating the residual mechanical stresses in the sample and the modification of its microstructure, which can lead to the reduction of the destruction threshold for the next pulse. Using the microphotographs (Figs 3c, 3f) the radial profiles of the brightness distribution were plotted that correspond to the induced Δn [curve (*1*)] and the residual [curve (*2*)] stress in the vicinity of the filament (Fig. 3g).

According to Fig. 3g, the modified region is much larger than the destructed region and the region of the induced refractive index. The obtained dependences have maxima near the filament walls. Directly in front of the damaged region tip one can also observe (see Figs 3a, 3d) a cylindrical segment 7–10 μm long with increased brightness and residual mechanical stress. Such is the general picture of the sample structure modifications after the impact of spatially separated single pulses: the destruction channel is surrounded by the cladding with the induced Δn and the larger-size region of modified microstructure.

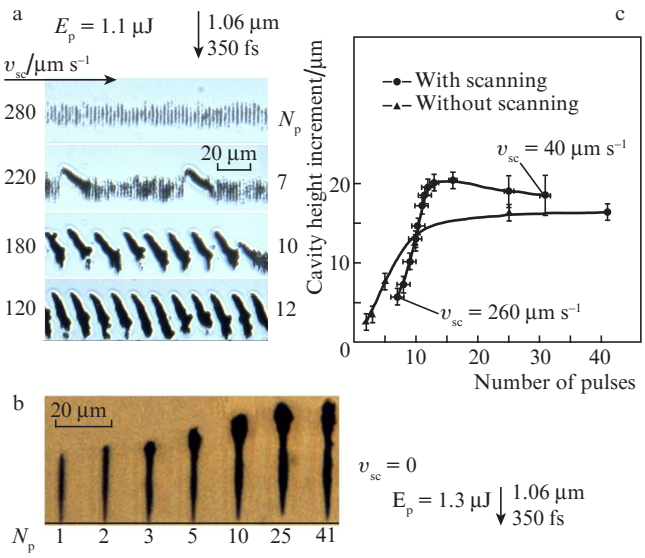

Figure 4. Microphotographs of the intra-volume destruction of the PC sample, produced by FS pulses at different scanning velocities (E_p = 1.1 μJ; f =100 Hz) (a) and at $v_{sc} = 0$ (E_p = 1.3 μJ) (b), and the dependence of the total increase in the destruction region length on the number of pulses N_p in a single cycle (c).

3. Formation of cyclic intra-volume spatial patterns

A different picture is observed when the scanning of the sample is performed with the overlap of the radiation focusing spots. It is well known [23] that the degree of the overlap plays a crucial role in micromachining of virtually any material. To determine the role of this parameter in our case, the following experiment was organised. The sample was mounted on the translation stage (see Fig. 1) and was moved perpendicular to the radiation beam from left to right with a discrete set of velocities v_{sc} = 280–40 μm s^{-1}. The repetition rate of FS pulses was f = 100 Hz, the pulse energy E_p = 1.1 μJ, and the depth of focusing into the sample was $f_d \approx 1$ mm. Figure 4 presents the traces of the impact of FS pulses for different v_{sc} in the form of inclined cavities of destruction in the samples of polycarbonate. The velocity v_{sc} in every row is constant, and the energy E_p is constant for all rows (Fig. 4a).

The analysis of this figure reveals a set of features, characteristic for the studied regime. In the course of sample scanning with every new pulse the destructed region also shifts towards the objective, then returns to its initial position (at the depth f_d), and then a new cycle begins. The number of pulses, involved in one cycle, i.e., in the formation of one cavity, decreases with increasing scanning velocity. The length of each cavity also decreases with increasing v_{sc}, and the angle of inclination of these internal cavities with respect to the scanning direction decreases with increasing v_{sc}.

Figure 4c presents the increase in the destruction region length Δz per one cycle in comparison with the initial length of the damage under the action of a single pulse (line 280 μm s^{-1} in Fig. 4a), when the interaction of filaments is absent. In this case, the total cavity length may exceed the length of the initial filament by more than two times. For $v_{sc} = 0$ the filament length quickly grows (during 9–10 pulses), then the growth of the destructed region length is saturated, with a simultaneous increase in its cross section, the length of the filament becoming almost constant. For comparison in Figs 4b and 4c the traces of the destructed region in the absence of scanning and the dependence of the destructed region length growth on the number of pulses N_p are presented.

4. Discussion of the results

Because in this experiment we varied only the parameter v_{sc}, it is obvious that all observed phenomena are related to the parameter $\delta x = v_{sc}/f$. It is known that the FS pulses, focused into the sample, can cause different modifications of the material structure, such as the complete destruction of the material in the region of the waist, the depolymerisation, the increase in the substance density, etc. [24, 25]. Due to these modifications the optical characteristics of the material (absorption, scattering and refraction of light) are changed, the optical anisotropy appears due to the residual mechanical stresses, and the breakdown threshold is reduced as a result of the structure changes and partial destruction of the material in the immediate proximity of the filament [26, 27]. Figures 3 and 5 present the photos that confirm these considerations. Figure 5a is of particular interest, since in it the filament is clearly seen, surrounded by a cladding with higher brightness of the glow, and the bright fringes, which are, obviously, waveguides (Fig. 5d).

To develop the technologies of fabricating intra-volume reproducible patterns (or the technologies of their suppression) it is important to understand how the next pulse of the focused radiation acts on the modification, produced in the material by the previous pulse. In Fig. 6 the possible schemes of such interaction are presented for the cases $v_{sc} = 0$ (a) and $v_{sc} \neq 0$ (b, c, d). After the impact of a FS pulse the region of destruction appears in the sample, having the shape of a filament with the diameter of the order of 2 μm, surrounded by the cladding with an increased density $\Delta\rho$ [28] and refractive index Δn (Fig. 5a), in turn, surrounded by the larger-diameter cladding with the modified microstructure, which is confirmed by the presence of residual stresses (Figs 3d–f). Such a view does not contradict the results of Refs [28–30], in which it was shown that in the process of fabricating Bragg struc-

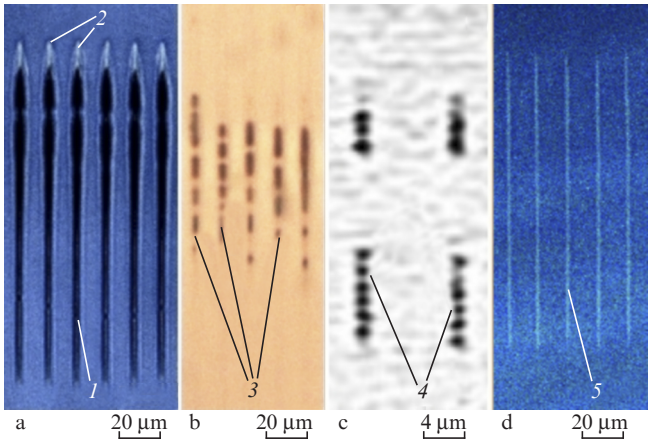

Figure 5. Material structure modification under the impact of single FS pulses on the PC (a, d), PMMA (b) and fused silica (c). The destruction regions having the shape of a filament (*1*), the changes in the refractive index beyond the destruction zone (*2*), the boundary between the liquid (MMA) and gaseous (in the form of meniscus) phase (*3*), the chains of destruction regions in the form of hollow spheres (*4*) and the intravolume waveguide patterns (*5*) are presented.

tures and waveguides in bulk samples of polymethyl methacrylate (PMMA), polycarbonate (PC) and other polymers the main contribution to the variation Δn is due to the variation of density and the structure modifications of the material.

At present the quantitative data on the variation Δn under the action of FS pulses are insufficient. However, in Refs [31, 32] the variations Δn in PC up to 1×10^{-4} are reported (under the same conditions in PMMA $\Delta n \approx 0.4 \times 10^{-4}$); moreover, in PMMA, which is similar to PC in physical and optical properties, by choosing the experimental conditions the variation Δn from 0.4×10^{-4} to 4×10^{-3} can be achieved [33–35]. Using these data and the optical scheme, presented in Fig. 6, we calculated the elongation ΔL of the cavity for different shifts of the sample with respect to the objective axis and without the shift. In these estimative calculations, aimed at the qualitative explanation of the experimental results, the value $\Delta n \approx 2 \times 10^{-3}$, belonging to the range of Δn variations mentioned above, provided the best agreement with the experimental results. From Fig. 6a it is seen that for $v_{sc} = 0$ the most part of the rays, belonging to the second pulse and the following ones, are focused into the destroyed region, where they are absorbed almost completely, thus increasing the region diameter.

In the presence of a shift (Figs 6b–d) the main part of the rays are focused in the region with the modified refractive index Δn, which leads to additional focusing, change of ΔL, and formation of hollow patterns with different slope, the slope angle decreasing with the growth of v_{sc} and δx. We should note that such values of ΔL are obtained without the allowance for the material structure modifications and their spatial configuration at the interface with the cavity, which can reduce the breakdown threshold in this region, increase the size and change the shape of the destructed region after the impact of the next pulse. From Fig. 4b it is seen that for the number of pulses $N_p \geqslant 2$ the filament cross section increases, particularly in its head part, and, therefore, its shape changes. For $N_p \geqslant 5$ this process becomes dominant, which, probably, leads to the saturation of the filament length growth and then to the growth termination at $N_p \geqslant 40$ (Fig. 4c). This behaviour is, probably, related to the fact that the abovementioned claddings with increased Δn (Fig. 5a) and $\Delta\rho$, as well as the change in the material microstructure, possess complex spatial configuration and correspond to a more complex distribution of the radiation intensity and density of electrons in the region of the geometric focus, e.g., such as in Ref. [27] (Fig. 7).

The self-induced shift of the damage region produced by the FS laser radiation inside the sample under the conditions

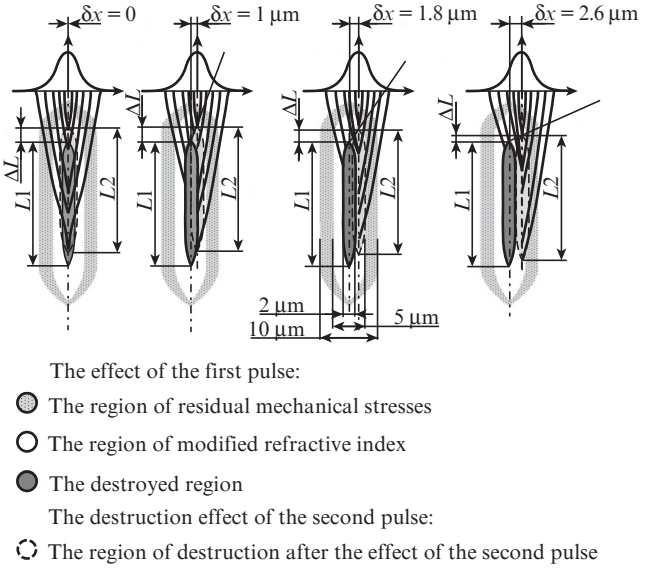

Figure 6. Hypothetic scheme of formation of inclined cavities: material modification under the action of the first FS pulse and the path of rays under the focusing of the second Gaussian pulse without (a) and with the displacement (b, c, d): $L1$ is the length of the cavity, produced by the first pulse; $L2$ is the length of the cavity, produced by the second pulse; ΔL is the increment of the cavity length.

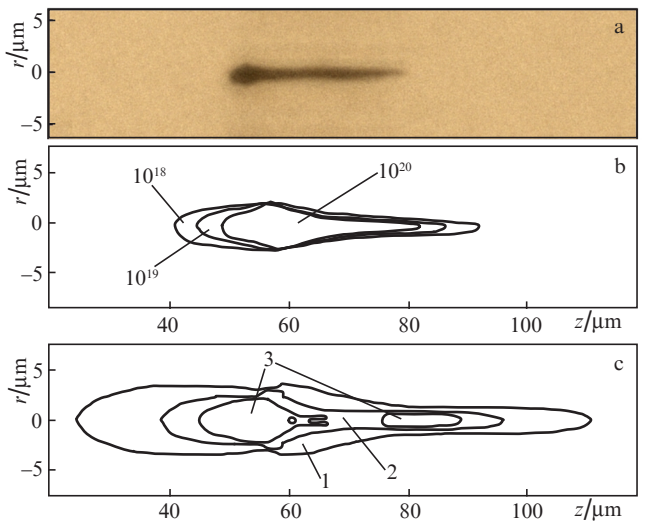

Figure 7. Comparison of experimental and theoretical results: a photograph of the cavity, produced by three pulses in PC (1025 nm, 350 fs, $E_p = 1.3$ μJ, 100 Hz, NA = 0.39) – the present work (a); numerical simulation (the curves are isolines of the concentration of electrons 10^{18}, 10^{19}, 10^{20} cm^{-3}) with 800 nm, 160 fs, NA = 0.5, 1 μJ (b); numerical simulation (the curves are isolines of the energy flux density 1, 2 and 3 J cm^{-2}) with 800 nm, 160 fs, NA = 0.5, 1.1 μJ (c). The calculated data for silica are borrowed from Ref. [27].

of its scanning is also observed in the case of high-frequency (0.5 – 2 MHz) micromachining regimes. Figure 8 presents the photographs of microdestructions in PC after using the laser with $f = 2$ MHz, $\tau_p = 300$ fs, $E_p = 150$ nJ. It is seen that the situation resembles that for low frequencies, but the essential differences are present. For example, the number of pulses in the cycle for $f = 2$ MHz is almost by 100 times greater than for $f = 100$ Hz; the increment Δz for these values of f has a maximum at $\delta x \sim 0.02$ and 1 μm, respectively (Fig. 9). The structures can have the shape of drops, blots, bridges with the melted-looking contours, so that the most probable mechanism of their formation is a thermal one. Indeed, for PC with the heat diffusion coefficient $D \approx 1.43 \times 10^{-7}$ m^2 s^{-1} [36] the time of heat removal from the volume with the diameter $d \sim 2$ μm is $\tau_D = d^2/4D \approx 7 \times 10^{-6}$ s [23].

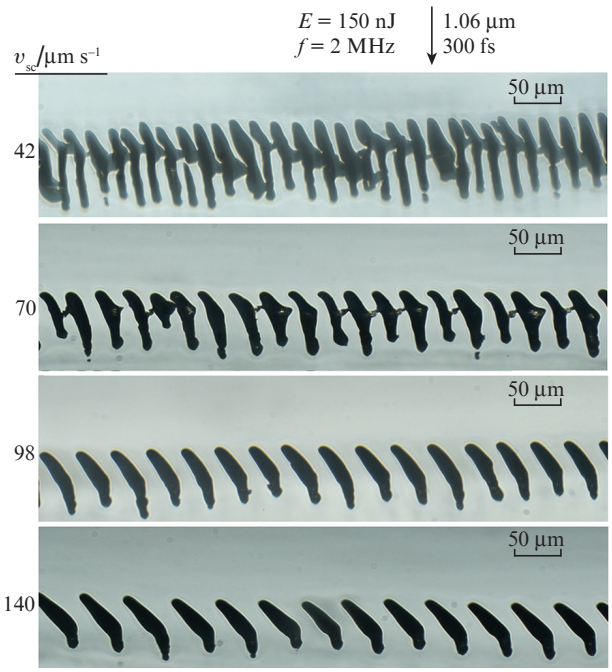

Figure 8. Microphotograph of intra-volume destructions of the PC sample by FS pulses at different scanning velocities; NA = 0.39.

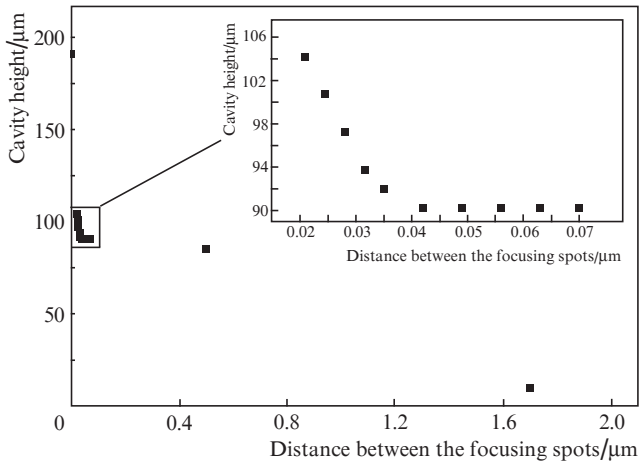

Figure 9. Dependence of the cavity height on the distance between adjacent focusing spots; NA=0.39, $E_p = 150$ nJ, $f = 2$ kHz.

Thus, if $f \ll 1$ MHz, then all thermal processes have time to be finished before the arrival of the next pulse, and this regime practically does not differ from the single-pulse one. For high frequencies f the situation is different. If the energy E_p is equal to the threshold energy or even smaller than it, then the heat, transferred to the focal volume, has no time to diffuse and begins to be accumulated, the temperature of the focal volume grows, and the energy, released from it, heats and melts the adjacent microregions.

The use of the ideas about the formation of cycles in the case of sample scanning in the high-frequency regime of processing and the careful choice of experimental conditions made it possible to create in the PC sample a microcapillary, perpendicular to the optical axis. Figure 10 presents such a hollow structure, fabricated at $f = 500$ kHz, $v_{sc} = 600$ μm s^{-1} and the pulse energy, reduced to 120 nJ. It is seen that the capillary is a result of overlapping of a huge number of oblique sub-micrometre cavities, arising at the self-induced shift of the destruction spot towards the objective, maximal for the present conditions.

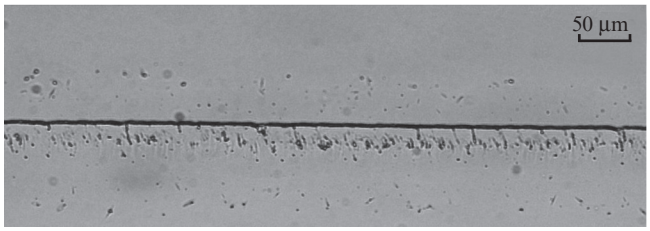

$f = 500$ kHz, $E_p = 120$ nJ

Figure 10. Microphotograph of a microcapillary; $f = 500$ kHz, $E_p = 120$ nJ, $v_{sc} = 600$ μm s^{-1}, NA = 0.39.

The results of the performed study were used for implementation of precision cutting and scribing of transparent dielectrics with a FS laser (Figs 11, 12). The polymer coronary stent made of poly(L-lactide) (PLLA) with the diameter 1.4 mm was cut helically (Fig. 11a). The quality of the cut can be evaluated from Fig. 11b. The 3-mm-thick PC sample (Fig. 12a) was cut into two parts. The width of the cut amounted to 4 μm. The roughness of the surface was $R_z \leqslant 1.5$ μm. Using the same technique the samples of silica optical BK7 glass

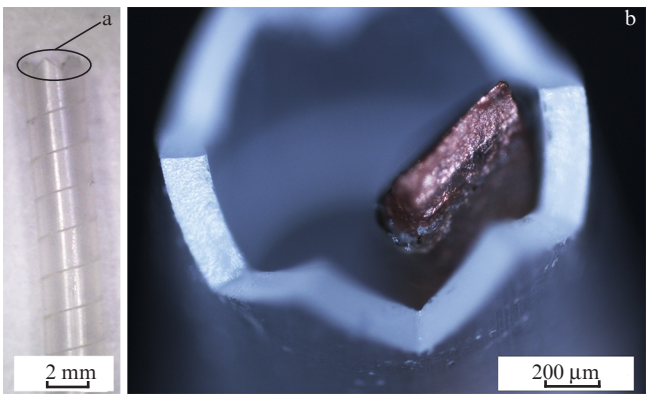

Figure 11. Photograph of the helically cut PLLA polymer medical coronary stent; $E_p = 40$ μJ, $f = 2$ kHz, $v_{sc} = 800$ μm s^{-1}, NA = 0.39.

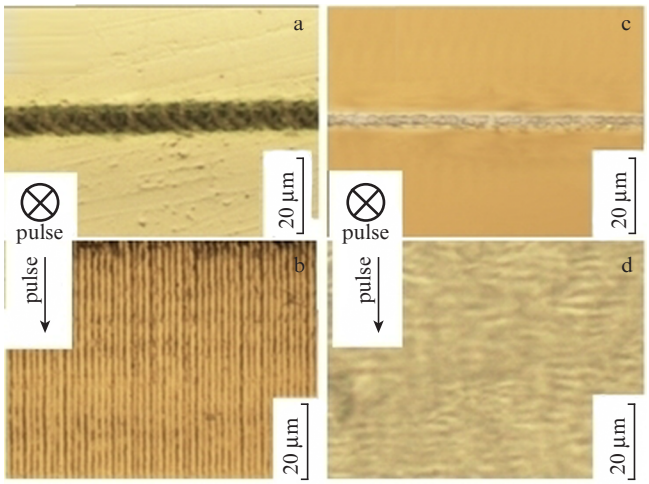

Figure 12. Microphotographs of the PC sample cut. The sample thickness is 3 mm, the cut width is 4 μm [top view of the cut (a) and its surface (b)], and the BK7 glass with the thickness 1.03 mm, the cut width 2 μm [top view of the cut (c) and its surface (d)]; E_p = 10 μJ, NA = 0.545, v_{sc} = 800 μm s^{-1}, f = 200 Hz.

were cut (Fig. 12b), the surface roughness was $R_z \leqslant 2.5$ μm. The highest-quality cut is achieved under such experimental conditions, when the cyclic regime of destruction does not occur.

Thus, the versatile use of the results of the performed studies in the transparent materials micromachining technology and the choice of the optimal experimental parameters for every material allow the improvement of the cut quality.

5. Conclusions

By scanning transparent materials with FS radiation having appropriately chosen parameters one can implement different regimes and obtain different results of materials processing. Thus, the scanning with a single spatially separated pulse having an energy near the breakdown threshold leads to the formation of a number of separate filaments or waveguides, oriented along the beam direction. When the sample is scanned with the pulses having the energy, smaller than that of the destruction threshold, but under the considerable overlap of the focusing spots, the line cavities directed perpendicular to the laser beam are formed. We investigated the occurrence conditions and determined the characteristic indicators of the intermediate regime, in which in the process of the sample scanning the region of damage at each next pulse is shifted also towards the objective, and after reaching some limit value returns to the line of the geometric focus, forming an intra-volume hollow periodical pattern. The main condition for the occurrence of the described regime is the hitting of the focusing spot of each next pulse into the microregion of irreversible material modifications, produced by the previous pulse. It is supposed that the damage region displacement under the irradiation with subsequent pulses and the occurrence of such a regime is caused mainly by a change in the refractive index and the reduction of the breakdown threshold due to a change in the material density $\Delta\rho$ and structure in the microregion, adjacent to the wall of the cavity, produced by the previous pulse.

It is shown that the results of the performed study can be used in the technology of high-precision cutting, scribing and fabricating different patterns inside transparent dielectrics (PC, PLL, fused silica) using the FS laser radiation. The best processing quality is achieved in the absence of cyclic regime.

Acknowledgements. The authors express their gratitude to A.S. Suvorina for the help in conducting the experiments.

References

1. Gattass R.G., Mazur E. *Nature Photon.*, **2**, 219 (2008).
2. Farson D.F., Choi H.W., et al. *J. Micromech. Microeng.*, **18**, 035020 (2008).
3. Kim T.N., Campbell K., et al. *Appl. Phys. Lett.*, **86**, 201106 (2005).
4. Gomez D., Tekniker F., et al. *Opt. Eng.*, **44**, 051105 (2005).
5. Li X., Hofmeister W., Shen G., Davis L., Daniel C. *Proc. Materials and Processes for Medical Devices (MPMD) Conference and Exposition* (Palm Desert, USA, 2007).
6. Stuart B.C., Feit M.D., et al. *J. Opt. Soc. Am. B*, **13**, 459 (1996).
7. Schaffer C.B., Brodeur A., et al. *Opt. Lett.*, **26**, 93 (2001).
8. Burakov I.M., Bulgakova N.M., et al. *J. Appl. Phys.*, **101**, 043506 (2007).
9. Nikumb S., Chen Q., Li C., Reshef H., Zheng H.Y., Qiu H., Low D. *Thin Sol. Films*, **477**, 216 (2005).
10. Davis K.M., Miura K., et al. *Opt. Lett.*, **21**, 1729 (1996).
11. White Y.V. et al. *Opt. Express*, **16**, 14411 (2008).
12. White Y.V., Parrish M., Li X., Davis L.M., Hofmeister W. *Proc. SPIE Int. Soc. Opt. Eng.*, **7039**, 70390J (2008).
13. Toratani E., Kamata M., Obara M. *Appl. Phys. Lett.*, **87**, 171103 (2005).
14. Lenzner M., Kruger J., et al. *Rev. Lett.*, **80**, 4076 (1998).
15. Gattass R.R., Cerami L.R., Mazur E. *Opt. Express*, **14**, 5279 (2006).
16. Glezer E.N., Mazur E. *Appl. Phys. Lett.*, **71**, 882 (1997).
17. Pu J., Zhang H. *Opt. Commun.*, **151**, 331 (1998).
18. Karman G.P., Van Duijl A., Woerdman J.P. *J. Mod. Opt.*, **45**, 2513 (1998).
19. Sun Q., Jiang H., et al. *Opt. A: Pure Appl. Opt.*, **7**, 655 (2005).
20. Watanabe W., Tome T., Yamada K., Nishii J., Hayashi K., Itoh K. *Opt. Lett.*, **25**, 1669 (2000).
21. Sowa S., Watanabe W., Nishii J., Itoh K. *Appl. Phys. A: Mater. Sci. Proc.*, **81**, 1587 (2005).
22. Saerchen E., Liedtke S., Schlage F., Will F., Lubatschowski H. *Proc. SPIE Int. Soc. Opt. Eng.*, **8803**, 880305 (2013).
23. Lubatschowski H., Rathjen C. Patent № US20070055221 (2007).
24. Schaffer C., Brodeur A., Nishimura N., Mazur E. *Proc. SPIE Int. Soc. Opt. Eng.*, **3616**, 143 (1999).
25. Juodkazis S., Nishimura K., et al. *Phys. Rev. Lett.*, **96** (16), 166101 (2006).
26. Liu D., Li Y., Liu M., et al. *Appl. Phys. B*, **91** (3–4), 597 (2008).
27. Couairon A., Sudrie L., Franco M., Prade B., Mysyrowicz A. *Phys. Rev. B*, **71**, 125435 (2005).
28. Poumellec B., Lancry M., et al. *Opt.Mater. Express*, **1**, 766 (2011).
29. Mochizuki H., Watanabe W. *Appl. Phys. Lett.*, **92**, 091120 (2008).
30. Zoubir A., Lopez C., et al. *Opt. Lett.*, **29**, 1840 (2004).
31. Mochizuki H. et al. *Thin Sol. Films*, **518**, 714 (2009).
32. Mochizuki H., Watanabe W. *Proc. SPIE Int. Soc. Opt. Eng.*, **7585**, 75850B (2010).
33. Sowa S., Watanabe W., et al. *Opt. Express,* **14**, 291 (2006).
34. Hirono S., Kasuya M., et al. *Appl. Phys. Lett.*, **94**, 241122 (2009).
35. Baum A., Scully P.J., et al. *Opt. Lett.*, **32**, 190 (2007).
36. Zhang X., Hendro W., et al. *Intern. J. Thermophys.*, **23**, 1077 (2002).